McNair Scholars Journal

Volume 14 | Issue 1 Article 8

2010

Transmission of Quantum Information via Laguerre Gaussian Modes

Aaron Schutza
Grand Valley State University

Table of Contents | *McNair Scholars 2010*

Transmission of Quantum Information via Laguerre Gaussian Modes

Aaron Schutza
McNair Scholar

Richard Vallery, Ph.D
Faculty Mentor

Abstract

A new era of technology is fast approaching in which quantum computation may become a reality. In the near future, technical applications may require a method of correlating two isolated quantum systems. This would require a signal carrier to be a quantum entity itself. We survey the quantum states of photons as a medium for encoding information. A communication scheme using the modulation of spatial modes and polarization states on free space or fiber optics is proposed. The Laguerre-Gaussian spatial mode is studied with these applications in mind. We also study photographic slide film as a means of creating diffraction gratings. Holographic diffraction gratings were created in order to generate Laguerre-Gauss beam modes of varying quantum number n. The spatial mode phase characteristics were then studied with a Mach-Zehnder interferometer.

1 Introduction

Modern technology is entrenched in the use of bulk material properties as a medium of information processing. As we scale down to smaller and smaller devices, heat generated by electrical current and the granularity of matter limit the density of circuit elements. Researchers currently strive to overcome these limitations for the continued evolution of technology required by countless scientific, industrial and commercial applications. Since the current paradigm of information processing faces physical limitations, other computational schemes may be fruitful in attaining higher information density and processing speed. As we approach the scale of the atom, there is a new set of phenomena and physical properties that become available.

1.1 Quantum Computation

Modern computers almost exclusively make use of electrical voltages and magnetic states of materials to process and store information. There has been little need to develop other means of computation since this paradigm has offered a multitude of circuit elements from which technological devices are built. At the scale of modern nano-technology, the physics of atoms and their constituent particles govern the properties of materials. In this regime, we can no longer rely on the bulk electrical properties of materials as a means of information processing. We are now interested in assigning information to the quantum states of atoms and subatomic par- ticles.

To achieve this task, we must consider two aspects of quantum systems called coupling and coherence [1]. The coupling of a system describes how corresponds to how

strongly it reacts to external forces. For instance, a strongly coupled system is sensitive to the state of its environment, while a weakly coupled system is less reactive to its surroundings. The more coupled a system is to its surroundings, the easier it is to measure and manipulate. The coherence of a system corresponds to how long it can stay in a particular quantum state. A system that is weakly coupled with its environment is able to achieve coherence for a longer time. We may think of these concepts in terms of the time evolution of a given system. The dynamics of our system is governed by the Schrödinger equation:

$$i\hbar\frac{d}{dt}|\psi\rangle = H|\psi\rangle. \tag{1}$$

The state of the system is $|\psi\rangle$, a vector of Hilbert space, and H is the Hamiltonian of the system. The Hamiltonian can be split into terms that correspond to the coupling of the system to its environment. If we wish to describe an external input that controls the state of the system, we could write $H = H_{in}(t) + H_{env}$ where H_{env} describes the system's interaction with its environment. $H_{in}(t)$ describes coupling of the system to the instruments used to manipulate it into a desired state and is generally a function of time. Systems in which H_{env} is small and $H_{in}(t)$ can be modulated quickly are desirable for use in quantum computation.

Experimental research has developed systems which retain their quantum state for a sustained period and can be manipulated by external forces. These are typically in environments that are extremely cold to reduce thermal agitations from the surroundings, minimizing H_{env}. Quantum dots are an example of solid state systems that allow the manipulation of the spin state of single electrons in an ultracold environment. More elaborate experiments are able to excite electrons to higher energy levels and force them to emit single photons. Modern experimental research has achieved the required precision and control of atomic and solid state systems to be applicable to information storage and processing.

If we are ever to use these atomic systems as a medium of computation, there will undoubtedly be a need for some way of communicating information between two of them. It won't be a simple matter of hooking up a phone line between the two. Any communication scheme applicable to quantum information must use quantum entities as signal carriers.

1.2 Quantum Information

In modern computer technology, often called classical computation or classical computers, information is stored and transmitted in binary strings. Each element of a string of information takes on only two distinct values, to which computer scientists have arbitrarily assigned 0 and 1. We are used to seeing strings of binary code, e.g., 10100010, which we will write as a list:

$$1,\ 0,\ 1,\ 0,\ 0,\ 0,\ 1,\ 0.$$

This serves as the basis of all digital computer processing. With quantum computers, we are now interested in carrying out computations involving the *superposition* of quantum states.

Quantum information now has us thinking in terms of a different mathematical entity altogether. Instead of communicating information with digits, that is, binary 1's and 0's, we ascribe it to *kets*. In quantum mechanics, the state of the system $|\psi\rangle$ is a ket belonging to the set of all available states of the system. This set of kets spans Hilbert space, which is the set of all kets of finite norm. If a ket is not a member of Hilbert space, it can't represent a physical system. We often choose a basis in Hilbert space that is constructed from eigenkets in order to understand the state in terms of physical observ-

ables. We must pick a set of compatible observables to build an eigenbasis out of the tensor product of the subspaces that their eigenkets span. Consider an observable A and eigenspectrum $\mathbb{A}$. The eigenvalue problem reads

$$A|n\rangle = a_n|n\rangle,\ a_n \in \mathbb{A}.$$

If we choose the set of eigenkets $|n\rangle$ as an orthonormal basis in Hilbert space, then the expansion postulate states

$$|\psi\rangle = \sum_n c_n|n\rangle \tag{2}$$

for any $|\psi\rangle$ of finite norm [2].

We now consider a system which has two conjugate states available to it. It now has a two dimensional Hilbert space such that the state

$$|\psi\rangle = c_i|i\rangle + c_j|j\rangle$$

is a linear combination of two eigenkets to some observable. We attribute the binary 1's and 0's of classical information to these conjugate kets:

$$1, 0 \Rightarrow |1\rangle, |0\rangle.$$

Note that in this notation, the numbers 1 and 0 do not correspond to any quantum number and are introduced by hand to correspond with classical computation. The state of a binary quantum system is now written

$$|\psi\rangle \Rightarrow |\text{qubit}\rangle = c_0|0\rangle + c_1|1\rangle. \tag{3}$$

Now the system is said to be an element of information storage and transfer, and Equation (3) is called a binary quantum digit (qubit).

In quantum computation and communication, we encode information in strings of qubits instead of bits, which may be written as

$$a_0|0\rangle + a_1|1\rangle,\ b_0|0\rangle + b_1|1\rangle,\ c_0|0\rangle + c_1|1\rangle,\ \ldots$$

In this scheme, we are using qubits as a means of information transfer and processing.

Quantum computation and communication offer many advantages over classical computers because of its use of qubits. There are various new algorithms that use the qubit to solve problems that would take a classical computer an exponentially longer time to compute [1]. Quantum Cryptography makes use of the qubit to send ultra secure signals that can't be intercepted by a third party. The advantages of using quantum information give a great incentive to pursue physically realizable communication methods.

2 Theory

Light presents itself as a prime candidate for communicating quantum information. Photons could be used as quantum signal carriers because they're quantum particles and have a variety of states available to them. We look to the use of photons in quantum information transfer between two isolated quantum systems. We now develop a basis of states for which the spin and orbital angular momentum observables are compatible.

2.1 Angular Momentum Eigenstates

If we are to find a physical system that could represent a qubit, Equation (3) has us looking for quantum objects that possess an observable with at least two distinct eigenstates to which we can assign the logical 0 and 1. Either a single or multi-particle system could have this desired property. We focus our attention to the single particle case. The intrinsic spin of fundamental particles is a perfect candidate observable. The components of the spin operator $\mathbf{s}$ do not commute, so we can't build an eigenbasis involving more than one of them. In cartesian

coordinates, the spin operator is written

$$\mathbf{s} = s_1\mathbf{e}_1 + s_2\,\mathbf{e}_2 + s_3\mathbf{e}_3$$

where its components have the commutation relation

$$[s_i, s_j] = i\hbar\epsilon_{ijk}s_k \tag{4}$$

and ϵ_{ijk} is the Levi-Civita symbol [2]. With this commutation relation, it can be shown that $[\mathbf{s}^2, \mathbf{s}] = 0$, which means that the squared norm of the spin vector and any one of its components commute. If we form a common eigenbasis of $\mathbf{s}^2$ and one of its components s_i, we have

$$\begin{aligned} s_i|m\rangle &= m\hbar|m\rangle \\ \mathbf{s}^2|s\rangle &= s(s+1)\hbar^2|s\rangle \end{aligned} \tag{5}$$

and we may now write the state of a particle in the common basis $\{|m\rangle \otimes |s\rangle\}$ such that

$$|\psi\rangle = \sum_{m,s} c_{m,s}|m\rangle \otimes |s\rangle.$$

In the standard model of physics, the quantum number s in Equation (5) is empirically fixed at a single half integer value which depends on the particle being described. From Equation (4) it can be shown [2] that

$$m \in \{\, -s,\ -s+1,\ \ldots\ ,\ s-1,\ s\}. \tag{6}$$

This places a fundamental limit on the number of internal states available to a single particle. Nonetheless, any $s \neq 0$ would suffice in giving us two or more internal states in which to assign logical digits. One could imagine a communication scheme in which a stream of particles is sent between two locations while modulating the spin state in a chosen axis. Particles may acquire an orbital angular momentum (OAM) in addition to spin. The OAM operator $\boldsymbol{l}$ is a vector whose components have similar commutation relations to (4) which are written $[l_i, l_j] = i\hbar\epsilon_{ijk}l_k$. Proceeding in the same fashion, a common eigenbasis may be constructed for both $\boldsymbol{l}^2$ and one of the components l_i:

$$\begin{aligned} l_i|n\rangle &= n\hbar|n\rangle \\ \boldsymbol{l}^2|l\rangle &= l(l+1)\hbar^2|l\rangle \end{aligned} \tag{7}$$

where the basis would be $\{|n\rangle \otimes |l\rangle\}$. The total angular momentum of the system is then

$$\mathbf{j} = \boldsymbol{l} + \mathbf{s}.$$

We are interested in these additional quantized OAM states as a means of increasing the amount of logical states that could be assigned to an individual particle. The commutator algebra allows the quantum number l in (7) to be any half integer value, but we are limited to integer values because we require that our field to be single valued upon a rotation of 2π [2].

2.2 Communicating with Photon States

Digital communication with light has primarily relied on the classical aspects of radiation, such as amplitude and frequency. To be applicable to quantum information, we have to use the quantum mechanical aspects of the field. Photons are the quantized states of the electromagnetic field and are considered fundamental particles with a spin quantum number $s = 1$. According to (6), this allows for three distinct values of m. For a photon, a particle of zero rest mass, there is no eigenstate for $m = 0$ that is a solution to the field equations [2]. This leaves us with two spin states corresponding to $m = 1$ and $m = -1$ on an axis that is parallel with the propagation of the wave. For an integer spin field of zero rest mass, only the spin component in the direction of propagation $\boldsymbol{k}/k$ is compatible with the momentum operator $\mathbf{p} = \hbar\boldsymbol{k}$ [3]. Unlike other particles, the spin states of a photon have a correspondence to a classical aspect of light. The polarization of light can be understood in terms of these quantized spin states. If a wave is traveling

in a direction $\mathbf{e}_k = \boldsymbol{k}/k$, there are two independent spatial axes which are perpendicular to the wave vector $\boldsymbol{k}$. Let's consider a wave train of monochromatic light propagating in the $\mathbf{e}_k$ direction. We may write the electric field in terms of Cartesian coordinates, choosing the z-axis parallel with $\mathbf{e}_k$, as

$$\mathbf{E} = E_x e^{i(kz-\omega t+\delta)}\mathbf{e}_x + E_y e^{i(kz-\omega t+\phi)}\mathbf{e}_y$$

where δ and ϕ are phase angles of the two harmonic waves. Here, $\mathbf{e}_x$ and $\mathbf{e}_y$ form a basis of two rectilinear polarizations with respect to $\mathbf{k}$. If the difference between δ and ϕ is an integer multiple of π, then the wave is said to be plane polarized [4]. This means that the electric field vector oscillates back and forth in a plane of constant orientation. If this difference is not equal to an integer multiple of π, then the light is said to be elliptically polarized [4]. This state has the electric field rotating at each point in space as the wave propagates.

Linearly and elliptically polarized light can be understood in terms of eigenstates of spin. The spin quantum number m in (5) is limited to $\{1, -1\}$ for the spin component s_z. We may write a basis of circularly polarized states as a linear combination of the two linear polarizations [2]. With $\mathbf{e}_x \times \mathbf{e}_y = \mathbf{e}_k$ we write

$$\begin{aligned} \mathbf{e}_+ &= -\frac{\sqrt{2}}{2}(\mathbf{e}_x + i\mathbf{e}_y) \\ \mathbf{e}_- &= \frac{\sqrt{2}}{2}(\mathbf{e}_x - i\mathbf{e}_y). \end{aligned} \tag{8}$$

Photon states in the basis of $\mathbf{e}_+$ and $\mathbf{e}_-$ are eigenstates of the spin components parallel with $\boldsymbol{k}$ [2]. From (8) we can see that linear polarization is really a linear combination of circular polarizations. Manipulation of the spin state of light is easily achieved, and communication methods involving qubits encoded in the polarization of light have been demonstrated [5]. The two spin states present a perfect medium for assigning logical 0's and 1's. The total angular momentum may also be used in a similar way and may in fact be a more efficient means of communication. The infinite number of total angular momentum states places no limit on information density of each photon. But if we wish to assign quantum information to the OAM eigenstates and spin states simultaneously, we encounter a problem. One may always build eigenstates for the $\mathbf{j}$ operator, but in general, a particle of $s = 1$ can never be in a pure state with well defined spin and OAM quantum numbers m and n due to the spin orbit interaction [6]. An analagous procedure which resulted in (6) for the spin operator can be carried out for $\mathbf{j}$, resulting in quantum numbers $j \in \mathbb{N}$ and $i \in \{-j, -j+1, \ldots, j-1, j\}$ [6]. If we are to use the spin states and OAM states simultaneously, we must resort to the paraxial approximation.

2.3 The Laguerre-Gaussian Spatial Mode

Paraxial optics is primarily used to describe the dynamics of coherent light beams, such as that produced by laser diodes. If an electromagnetic wave is propagating in a non-dispersive, isotropic, linear, and homogeneous medium, all field components may be described by a single scalar function $u(\mathbf{r}, t)$ that contains all the information of the field [7]. We can write the vector potential in terms of this scalar function

$$\mathbf{A}(\mathbf{r}, t) = A_0 u(\mathbf{r}, t)\mathbf{n}$$

where $\mathbf{n}$ is a linear combination of the vectors in (8). The electric and magnetic fields are then expressed as $\mathbf{E} = \frac{-1}{c}\frac{\partial \mathbf{A}}{\partial t}$ and $\mathbf{B} = \nabla \times \mathbf{A}$ [6]. To solve for $u(\mathbf{r}, t)$ we use separation of variables between $\mathbf{r}$ and t so that $u(\mathbf{r}, t) = u(\mathbf{r})e^{-ikct}$ and make the paraxial approximation to the Helmholtz equation along the z direction in cartesian coordinates:

$$\left(\frac{\partial^2}{\partial x^2} + \frac{\partial^2}{\partial y^2} - 2ik\frac{\partial}{\partial z}\right) u(\mathbf{r}) = 0. \tag{9}$$

A complete basis of solutions to (9) are the Laguerre-Gauss (LG) modes. They are written in cylindrical coordinates (r, θ, z) as

$$\begin{aligned} u_{np} = \frac{e^{in\theta}}{w}\sqrt{\frac{2p!}{\pi(p+|n|)}}\left(\frac{\sqrt{2}r}{w}\right)^{|n|} \\ \times L_p^{|n|}\left(\frac{2r^2}{w^2}\right)\cdot\exp\left(-\left(\frac{r}{w}\right)^2 - \frac{ikr^2 z}{2(z^2+z_R^2)}\right) \\ \times\exp\left(i2p + i(|n|+1)\arctan\frac{z}{z_R}\right) \end{aligned} \tag{10}$$

with $r = \sqrt{x^2+y^2}$ and $\theta = \arctan(\frac{y}{x})$, $w = \sqrt{1+z^2/z_R^2}$ is the beam radius, $2z_R$ is the Rayleigh range of the beam, and $L_p^{|n|}(\ldots)$ are the associated Laguerre polynomials with $p \in \mathbb{N}$ and $n \in \mathbb{Z}$ [6]. A photon that is in the state with a scalar field amplitude described by (10) can be interpreted as being in an eigenstate of the z-axis orbital angular momentum operator l_z. In cylindrical coordinates this is written as

$$l_z = \frac{\hbar}{i}\frac{\partial}{\partial\theta}.$$

We will rewrite (10) as

$$u_{np}(r,\theta,z) = f_{np}(r,z)e^{in\theta}$$

and it is obvious that

$$\begin{aligned} l_z u_{np}(r,\theta,z) &= \frac{\hbar}{i} f_{np}(r,z)\frac{\partial}{\partial\theta}e^{in\theta} \\ &= n\hbar\, u_{np}(r,\theta,z). \end{aligned} \tag{11}$$

The vector potential can finally be written as

$$\mathbf{A}(\mathbf{r},t) = A_0\sum_{np} c_{np}\, f_{np}(r,z)e^{-ikct+in\theta}\mathbf{n}_{np}$$

where $\sum_{np}|c_{np}|^2 = 1$.

In the formalism of quantum mechanics, we can rewrite the eigenvalue problem (11) in terms of kets where $u_{np} \Rightarrow |n,p\rangle$, and we write

$$l_z|n,p\rangle = n\hbar\,|n,p\rangle.$$

These eigenstates are normalized with the condition [6]

$$\begin{aligned} \langle n,p\,|\,n',p'\rangle &= \iint_{\mathbb{R}^2} u^*_{np}(x,y,z)u_{n'p'}(x,y,z)\,dx\,dy \\ &= \delta_{nn'}\delta_{pp'} \end{aligned}$$

and an observable A is represented in this basis as

$$\langle n,p\,|\,A\,|\,n',p'\rangle = A_{nn'pp'}.$$

We can now write a photon state $|\gamma\rangle$ in the paraxial approximation as

$$|\gamma\rangle = \sum_{n=-\infty}^{n=\infty}\sum_{p=0}^{p=\infty} c_{np}|n,p\rangle \tag{12}$$

which follows from the expansion postulate (2).

We now consider the spin operator acting on the LG modes. Because the eigenstates of the spin operator are the circular polarizations, the extension of our description of $|\gamma\rangle$ to include spin states is made easy by the fact that we separated the polarization and spatial characteristics of the beam when carrying out the paraxial approximation. Without the paraxial approximation, we wouldn't be able to write a common eigenbasis of spin and OAM because of the spin orbit coupling inherent to zero rest mass fields. The spin acts on the polarization vector $\mathbf{n}_{np} = (c_+\mathbf{e}_+) + (c_-\mathbf{e}_-)$ where $|c_+|^2 + |c_-|^2$. If we rewrite (8) as $\mathbf{e}_- \Rightarrow |-1\rangle$ and $\mathbf{e}_+ \Rightarrow |+1\rangle$, we can write our state in a common basis of spin and OAM

$$|\gamma\rangle = \sum_{m=-1,1}\sum_{n=-\infty}^{n=\infty}\sum_{p=0}^{p=\infty} c_{npm}|n,p\rangle\otimes|m\rangle. \tag{13}$$

This serves as the basis for a potential communication scheme in which quantum bits are assigned to the spin states, and additional information is assigned to the OAM quantum number and associated radial number p.

3 Experimental Methods

Optical vortices are a feature of the LG modes, and their properties have been intensely studied in the field of singular optics. We turn our attention to the spatial characteristics of these intriguing swirls of light. The LG modes have interesting phase characteristics that are best observed as a level set of the scalar field wavefronts plotted in 3 dimensions. The phase is singular along the axis of the beam at $r = 0$. Far from the central beam axis, the scalar field approaches a plane wave; but with each wavefront out of phase by π at diametrically opposing points of the paraxial plane. This gives a strange corkscrew pattern to the scalar field, shown in Figure 1.

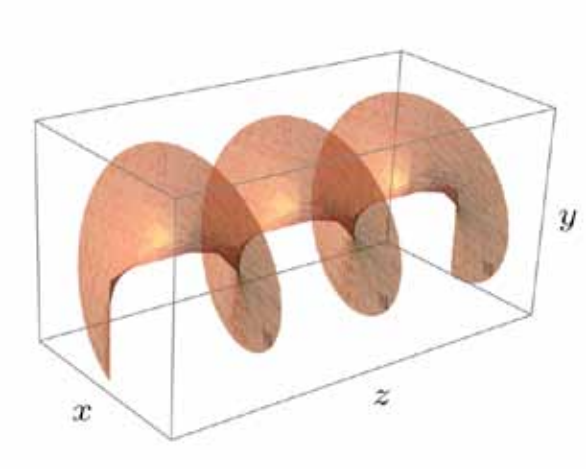

Figure 1: A level set of the scalar field phase for a u_{1p} mode. The plane represents a surface of similar phase, i.e., wavefronts. Notice the line of singular phase down the center of the beam. The presence of the singularity means that the field amplitude must approach zero along the axis of the beam.

When incident on a surface, the paraxial (plane perpendicular to propagation) intensity profile has a central area of zero intensity, giving it a doughnut like shape. Figure 2 shows a series of intensity profiles for various n. In order to better understand how LG modes are created and how they could apply to quantum information, we set out to make our own vortices in the lab.

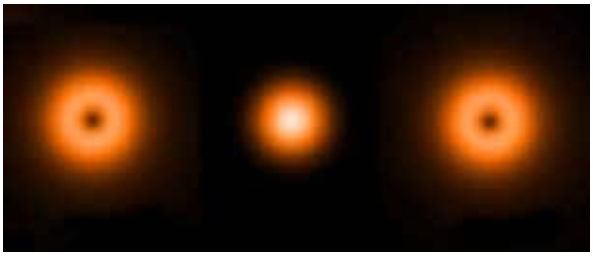

Figure 2: A plot of the intensity profile for an $n = -1, 0, 1$ from left to right. The $n = 0$ mode reduces to a Gaussian beam. The central hole in the others coincides with the axis of singular phase of the LG mode.

3.1 Computer Generated Holograms

We can experiment with LG modes by creating them via computer generated holograms (CGH). Scalar diffraction theory describes the field amplitude of light that is scattered by one of these diffraction gratings. Figure 3 shows an example of a CGH pattern that would produce our LG modes if laser light were to shine through its center. To make this, a density plot of the theoretical interferogram of an LG beam of OAM quantum number n and a Gaussian beam is calculated with the function [8]

$$I(x, y) = \frac{1}{2}\left[1 + \cos(2\pi x - n \arctan(y/x))\right].$$

The optical density would ideally be 100% where $I(x, y) = 1$, and 0% where $I(x, y) = 0$. We wish to put this pattern on a surface for which the black lines are optically dense and the white lines transparent to light. The light that passes through the transparent portion is diffracted and forms a holographic pattern. Figure 4 shows a diagram of this principle.

There are several techniques for transferring this pattern to a transparent medium. One could print it out on transparency film using a laser printer. A spatial light modulator could also be employed to create the density patterns. These two methods

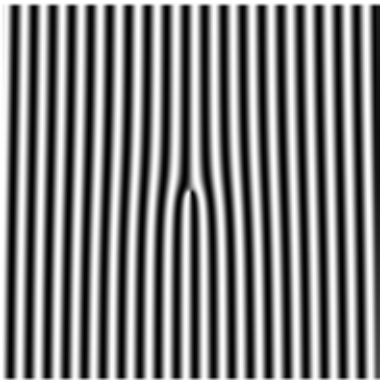

Figure 3: The computer generated hologram features a forked pattern with 1 dislocation made from the function $I(x, y) = \frac{1}{2}[1 + \cos(2\pi x - \arctan(y/x))]$. The pattern far from the origin looks like the line pattern $\frac{1}{2}(1 - \cos(2\pi x))$.

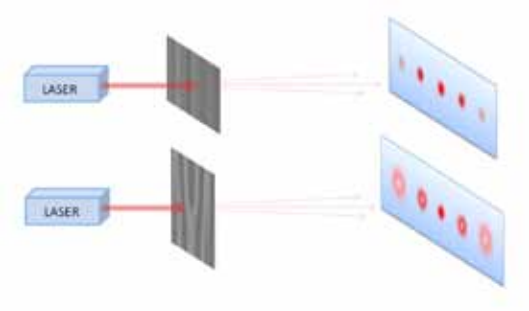

Figure 4: (Top) The familiar diffraction experiment. The diffracted patterns have no imprinted phase. (Bottom) A laser emitting a TEM_{00} shines down the center of the fork pattern. A diffraction pattern is seen on the other side with a Gaussian central mode and higher order LG modes that have the $e^{in\theta}$ imprinted in them. The order of the principal maxima coincides with the quantum number n. So, for example, an LG mode that is the second principal maximum of the pattern will have $n = 2$.

have a huge disadvantage in the resolution of the pattern that they can recreate. The resolution of a laser printer, typically 600dpi, makes it difficult to reproduce the CGH pattern without introducing aliasing. A spatial light modulator would face the same fundamental problem. Photographic film is a much more cost effective option and has a lot of flexibility. Photographic film negatives have been used before to create relatively high quality CGH's in an undergraduate laboratory [8]. We aimed to reproduce these results using photographic slide film instead. Figure 3 shows the part of the holographic pattern that was photographed. An SLR camera was loaded with Fujichrome Velvia 50, a daylight color reversal slide film with an ISO speed rating of 50. The fidelity of the pattern is limited only by the grain size of the exposure. The actual size of the grains of photographic film depends on the exposure time. This film has a diffuse RMS granularity value of 9, as measured by a standard micro-densitometer. A relatively low value for this rating means that a quick exposure will have small grain size. The graininess shows up as tiny speckles of higher optical density. If a pattern is too fine, then the film grain will drown it out.

To transfer the CGH pattern to our Fujichrome, we generated a large format, 100 MP digital density plot effectively 200 lines across using mathcad software. This pattern was printed with a 600dpi large format printer. The printout was then spray mounted to a flat surface, leveled, and photographed from a distance with the SLR camera. The shots were taken outside on a sunny day so that the pattern was illuminated by natural daylight. A large pattern with tight line spacing was needed because of the wide range of sizes the pattern would be on the film. If the pattern were too small, the far field of the incident laser mode would be cut off by the square edges of the pattern. A variety of focal lengths and exposure times was used for each frame. The slides that were studied in this investigation had exposure times ranging from 1ms to 2ms.

3.2 Creation of Laguerre-Gauss Beams

Out of the 36 exposures that were taken, a few were selected that exhibited appropriate contrast and line spacing. To measure the patterns created by the slides, a Hitachi HV-F31F 3 CCD color cam-

era was used. The CCD surface area is 4.77mm (horizontal) × 3.58mm (vertical) with a pixel spacing of 4.65µm per pixel. These specifications were used to measure the dimensions of the patterns that resulted from the slides. The laser that will make the pattern should be as close to the TEM_{00} mode as possible. We selected a Uniphase Model 1677 laser head that emits TEM_{00} with a mode purity of >95% to generate the diffraction patterns. The wavelength of the light was 594nm and had a beam diameter of 0.73mm. To capture a paraxial intensity pattern in the limit of Fraunhofer diffraction, the CCD was placed on a translation mount sufficiently far along the optical path length of the pattern that the principal maxima were well defined. The translation mount was set up to move the camera horizontally along the x-axis of the paraxial plane. The pattern was too wide to be captured in a single frame, so multiple images had to be overlayed. Each order captured was centered in the frame, and a total of four images were taken. They were compiled together with the GIMP using distance measurements from the translation mount. Figures 5 and 6 shows the compiled image.

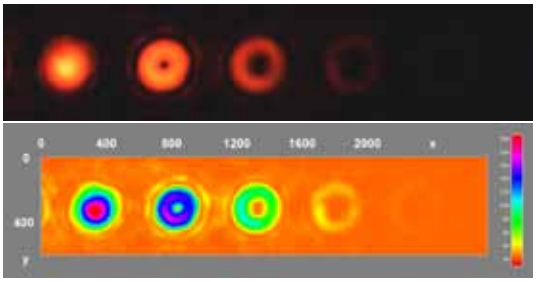

Figure 5: (Top) The resulting holographic pattern captured by panning the camera with a translation mount for the $D = 99.0$µm slide. (Bottom) The relative intensity of the captured image color altered for clarity. The legend on the right corresponds to the intensity relative to a saturation value of 255. The horizontal and vertical axes represent the (x, y) coordinates of the paraxial plane measured in pixels (4.65µm/pixel). The pattern is symmetrical about the axis of the central TEM_{00}, so only half the pattern was captured. From left to right are LG modes with quantum number $n = 0, 1, 2, 3, 4$. Distinct rings are visible around the central doughnut pattern of each mode. These are attributed to the number p, which characterizes the radial part of the u_{np} modes.

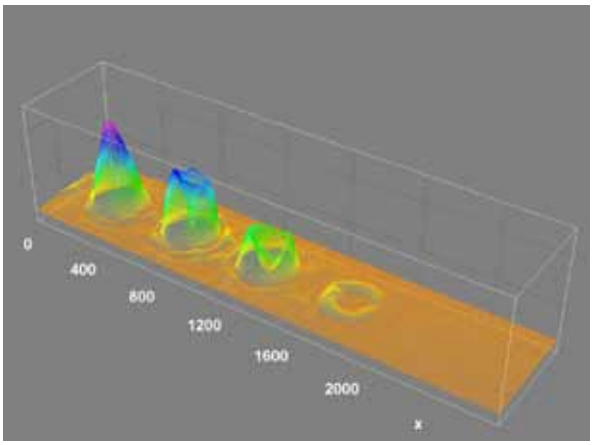

Figure 6: A 3 dimensional plot of the intensity for the $D = 99.0$µm slide. The color and height correspond to the relative intensity, and the displayed units are the same as in Figure 5.

A series of neutral density filters were used to attenuate the light to the range of sensitivity of the CCD. If the light was too bright, the higher intensity portions of the pattern would be cut off at the maximum relative intensity value of 255. To measure the dimensions of the holographic patterns, image analysis software was used to find the number of pixels between each principal maximum. To interpolate the center of the modes, a Gaussian blur filter was applied to the image shown in Figure 5 (Top) in order to smooth out maxima introduced by noise and film grain. This proved to be an effective method for finding the central axis of the LG modes and gave consistent maximal points for blur radii of 10 pixels and greater. When comparing the holographic patterns captured at different points along the optical path length, the angle between the central axis and principal maxima can be determined. Figure 7 compares the intensity of two such measurements. Using the formula

$$D \sin \theta_n = n\lambda$$

where D is peak to peak line spacing of the pattern on the slide, θ_n is the angle between the central axis and n^{th} principal maxima, and λ is the wavelength, the line spacing can be calculated from

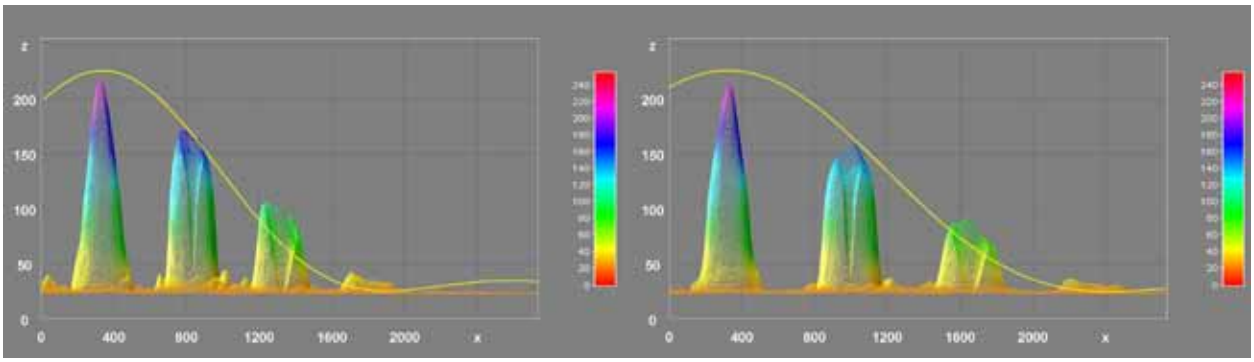

Figure 7: (Left) The intensity of the pattern plotted horizontally for the $D = 99.0\mu$m slide. The pattern was captured 38.9cm from the slide. (Right) The same plot for an image captured 51.6cm from the slide. Overlaid on both plots is the single slit irradiance calculated by the Fraunhofer integral evaluated with experimental measurements. The principal maxima of the diffraction pattern qualitatively follow this intensity profile.

the maxima spacing [4]. Using this technique, the slide that created the holographic pattern in Figure 5 was measured to have a line spacing of $D = 99.0\mu$m. Figure 8 features a holographic pattern that was created with a slide that had a higher line density. This slide was measured to have a line spacing of 39.9μm. The only modes visible for the $D = 39.9\mu$m were the first principal maxima.

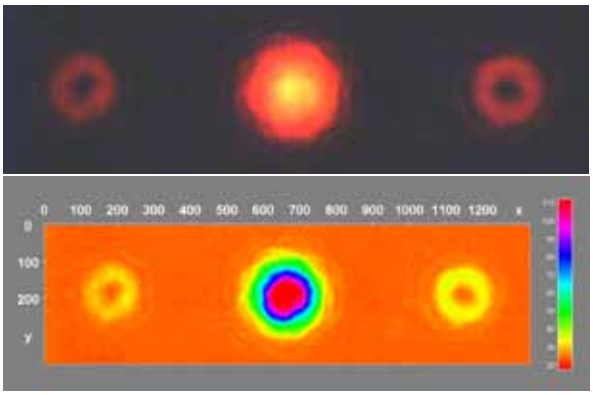

Figure 8: (Top) The diffraction pattern for the $D = 39.9\mu$m. The contrast has been altered to make the LG modes more visible. (Bottom) The original captures recolored. The only maxima visible correspond to $n = -1, 0, 1$ from left to right.

Compare Figure 8 with Figure 2 and you will notice that the experimental measurements have an extra ring around the central doughnut pattern. They are even more apparent in Figure 5. These are attributed to the radial number p in (10). The Laguerre polynomial determines how many radial rings there will be. The principal maxima of the holographic patterns are really linear combination of LG modes with different radial number p. We can interpret this in terms of (12) as an eigenstate of l_z expanded in states of differing radial number:

$$|n^{\text{th}} \text{ maxima}\rangle = \sum_{p=0}^{p=\infty} c_p |n, p\rangle.$$

The maxima of the slides, though not pure LG modes, have well defined quantum number n because of the degeneracy in p. We can write any eigenstate of l_z in this way.

3.3 The Mach-Zehnder Interferometer

In order to measure some of the characteristics of our LG modes, a Mach-Zehnder Interferometer (MZI) was constructed. Figure 9 shows our setup. The MZI consists of two cubic beam splitters and two mirrors arranged such that an incident beam is split 50:50. These two beams are then reflected by the mirrors into the second beam splitter where they intersect perpendicularly at the reflective interface. The dielectric coating at the interface of a beam splitter is situated so that one of the beams picks up a phase factor of π upon reflec-

tion while the opposing beam doesn't. This makes the transmitted and reflected beams at one output destructively interfere and at the opposite output constructively interfere. An MZI can be used as a means of measuring the quantum number n for an incident LG mode [9] as well as a variety of other interesting applications involving LG modes [10]. Figure 10 shows the LG mode measurement scheme devised in [9]. These applications consist of manipulating the state of the beam on either or both arms of the MZI and interfering them at the output. An example of this was carried out with our experimental setup. To see the mode purity of the first principal maximum for one of our slides, we captured the interferogram of the maxima and reference beam. This was achieved by inserting the hologram into one arm of the MZI and leaving the other unaltered. The interferance pattern that was captured is seen in Figure 11. The primary pattern is clearly visible as a discrete number of interference fringe dislocations at the top and bottom region of the pattern. If this procedure were carried out with the second principal maximum, we would observe two dislocations. In general the n^{th} maximum will produce n dislocations in the interferogram.

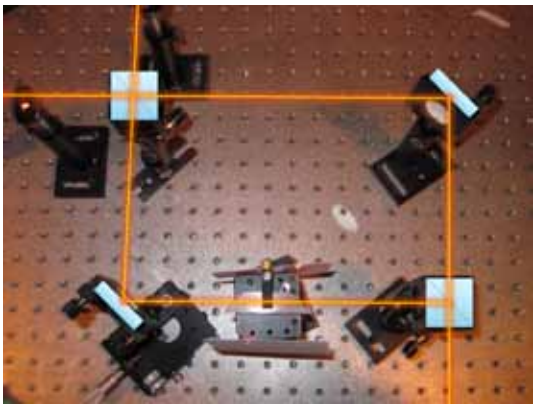

Figure 9: A snapshot of the MZI used in our experiment taken from above. The overlay demonstrates the symbolic representation of the beam splitters and mirrors. The beam splitters are the square boxes with a diagonal slash, and the mirrors are the rectangular boxes. A dove prism can be seen on one arm of the interferometer. Using two dove prisms, we could reproduce the sorting scheme carried out in [9].

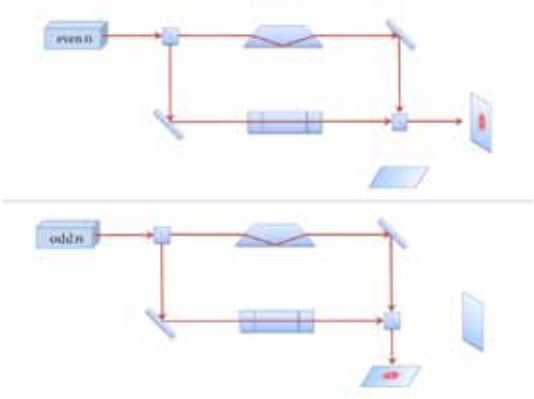

Figure 10: An MZI set up with dove prisms rotated by $\pi/2$ with respect to each other. The light coming in the MZI is interfered and LG modes with odd and even n exit the beam splitter perpendicularly provided that each arm has the exact same optical path length.

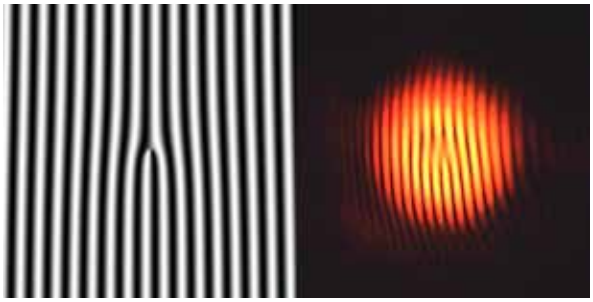

Figure 11: (Left) The theoretical interferogram of an LG mode of $n = 1$, and a plane wave. (Right) The interferogram of the first principal maximum of the $D = 99.0\mu$m holographic pattern interfered with a reference TEM_{00}. The radial distortion is due to the optical path length differences in each arm of the MZI imposed by using a diffraction grating. In addition to that, the beams have a different radius of curvature at the second beam splitter. These circumstances make it difficult to determine how much of the radial interference is attributable to the radial number p of the maximum being measured.

4 Discussion

To understand the manipulation of light in terms of quantum mechanics, we can think of the beam's interaction with optical elements in the context of paraxial evolution. If we rewrite the paraxial ap-

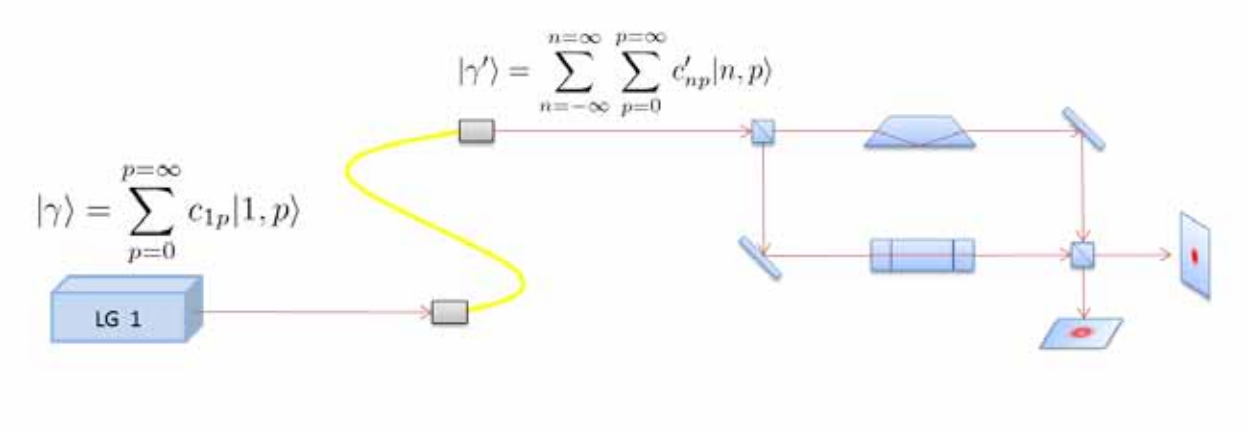

Figure 12: Fiber Distortion. This schematic represents how we can understand the paraxial evolution of the beam in terms of the eigenbasis we have constructed in (12). A prepared LG 1 mode is coupled to a fiber optic channel. The fiber distorts the output beam which can be seen as a transformation $|\gamma'\rangle = F|\gamma\rangle$.

proximation (9) as

$$\frac{1}{2k}\left(\frac{\partial^2}{\partial x^2}+\frac{\partial^2}{\partial y^2}\right)u(\mathbf{r}) = i\frac{\partial}{\partial z}u(\mathbf{r}), \qquad (14)$$

there is an apparent parallel with the temporal evolution of a quantum system governed by (1). The way that (14) is written may remind the reader of the wave mechanics for matter waves. While it is true that we associate the intensity of light with the probability of a photon arriving at a certain point in space, it is important to note the distinction between the scalar field amplitude and a position representation wavefunction. It is impossible to write a position vector operator that acts on the state space of photons and has components that commute [11][3]. This means we can only describe the probability of a photon arriving at a region of space in terms of the complex field amplitude. This seems counterintuitive at first, but it should make sense if one thinks of a photon as an excitation in a quantized field instead of a point particle. The intensity can then be thought of as the probability of the field quanta, i.e., photon, to interact with matter in a region of space [12]. If we wish to have a communication scheme with single photons, the intensity of the light must be sufficiently low to ensure that one photon at a time is traversing the optical path. We can then use (14) to describe the evolution of the photon state along the optical path. We can think of the coordinate along the axis of propagation in the regime of paraxial optics as an analog to the temporal parameter. The same ideas of coherence and coupling mentioned above could be applied to the paraxial evolution of a light beam. Coherence in this case would correspond to how far along the optical path length a photon would stay in a particular state. If we wish to guide the beam using an optical waveguide, it would undoubtedly distort the mode purity of an LG mode. Figure 12 shows this principle. Optical elements that produce as little distortion as possible are desirable for communication.

This study of the LG modes at Grand Valley State University has paved the way for many interesting opportunities for future undergraduate research. Future work will involve further investigation of the use of slide film in diffractive optics experiments. A study of the effect on fiber optics on LG mode purity could potentially be carried out. Future theoretical research would entail a more detailed analysis of the relationship between photon OAM and spin to determine the validity of (13).

References

[1] G. Fraser, editor. *The New Physics for the Twenty-First Century*. Cambridge University Press, New York, 2006.

[2] A. Messiah. *Quantum Mechanics*. Dover Publications, Mineola, New York, 1999.

[3] J. C. Garrison and R. Y. Chiao. *Quantum Optics*. Oxford University Press, New York, 2008.

[4] E. Hecht. *Optics*. Pearson Education Inc., San Francisco, CA, fourth edition, 2002.

[5] J.C. Boileau, R. Laflamme, M. Laforest, and C. R. Myers. Robust quantum communication using a polarization-entangled photon pair. *Phys. Rev. Lett.*, 93(220501), November 2004.

[6] E. Santamato. Photon orbital angular momentum: Problems and perspectives. *Fortschr. Phys.*, 52(1112), July 2004.

[7] J.W. Goodman. *Introduction to Fourier Optics*. Roberts and Company Publishers, Greenwood Village, CO, third edition, 2005.

[8] A.V. Carpentier, H. Michinel, and J.R. Salgueiro. Making optical vortices with computer-generated holograms. *Am. J. Phys.*, 76(10), October 2008.

[9] J. Leach, et al. Measuring the orbital angular momentum of a single photon. *Physical Review Letters*, 88(25), June 2002.

[10] Y.S. Rumala and A.E. Leanhardt. An angular phase grating based on optical vortex superpositions. Unpublished manuscript, May 2010.

[11] B. Skagerstam. Topics in modern quantum optics. arXiv:quant-ph/9909086 v2, November 1999.

[12] E. J. Galvez, et al. Interference with correlated photons: Five quatnum mechanics experiments for undergraduates. *Am. J. Phys.*, 73(2), March 2004.